Size dependence of structural, electronic, elastic, and optical properties of selenium nanowires: A first-principles study

Mousumi Upadhyay Kahaly,[a)] Prasenjit Ghosh,
Shobhana Narasimhan, and Umesh V. Waghmare
Theoretical Sciences Unit, Jawaharlal Nehru Centre for Advanced Scientific Research, Jakkur, Bangalore 560 064, India

(Received 13 August 2007; accepted 15 November 2007; published online 31 January 2008)

We have studied the structural, elastic, and optical properties of selenium nanowires, as well as bulk selenium, by performing first-principles density functional theory calculations. The nanowires are structurally similar to bulk trigonal Se, in that they consist of hexagonal arrays of helices, though there is a slight structural rearrangement in response to the finite size of the nanowires. These small structural changes result in Young's modulus decreasing slightly for progressively thinner nanowires. However, there is a significant effect on electronic structure and optical properties. The thinner the nanowire, the greater the band gap, and the greater the anisotropy in optical conductivity. The latter is due to the effects of finite size being much more marked for the case where the electric field is polarized perpendicular to the helical axis, than in the case where the polarization is parallel to *c*. For the case of bulk Se, we obtain good agreement with experimental data on the structure, elastic constants, and dielectric function.
[DOI: 10.1063/1.2824969]

I. INTRODUCTION

The great interest in one-dimensional nanostructures such as nanotubes and nanowires is partly driven by the possibility of their being used as active components in nanosized devices. Though carbon nanotubes and nanowires have attracted the majority of attention, selenium nanowires also offer intriguing possibilities. Bulk selenium has been used in applications such as photovoltaic cells, photocopiers, rectifiers, and xerography, because of its photoelectric behavior, optical activity, and linear and nonlinear optical properties.[1] The structure of trigonal bulk selenium, which consists of an array of one-dimensional helical chains, would seem to lend itself naturally to the formation of structurally similar selenium nanowires, which may conceivably possess, to a greater or lesser extent, the novel properties of the bulk material. The recent experimental syntheses of Se nanowires by laser ablation[2] and by a self-seeding solution process[3] have now made the development of nanoscale electronic or electrochemical devices[4,5] incorporating Se nanowires a real possibility.

In order to determine the feasibility of using selenium nanowires in technological applications, it is desirable to have an understanding of the electronic structure of these nanowires, as well as their mechanical stability. One would also like to understand how these properties vary with the diameter of the nanowires. We have performed first-principles density functional theory (DFT) calculations to investigate the structures as well as the elastic, electronic, and optical properties of a single helical Se chain ("Se-h"), a wire with one shell ("Se-w1"), consisting of six helical chains arranged around a central helical chain, and a wire with two shells ("Se-w2"), consisting of a further shell of 12 helical chains around Se-w1. We have also computed the properties of trigonal bulk Se. The unique position of selenium at the boundary of group VI in the Periodic Table between van der Waals molecular solids (O_2 and S_8) and covalent solids (Te) is manifested in the variety of its allotropic solid-state forms. Among these, trigonal bulk Se (*t*-Se) has a highly anisotropic crystal structure consisting of parallel helical chains stacked on a hexagonal lattice, with their axes parallel to the crystalline *c*-axis. The anisotropy in the crystal arises from a strong covalent bonding between neighboring atoms belonging to the same helix (intrachain bonding) and a relatively weaker interaction between neighboring atoms in adjacent chains (interchain bonding). Note that, unlike the case of carbon nanowires, in the case of selenium, due to the structural similarity between the nanowires and the bulk, one would expect that the properties of the nanowires should go over smoothly to that of the bulk, as one assembles nanowires of larger diameter by adding additional shells of Se helices. Thus, this system offers an interesting angle on understanding the effects of dimensionality on properties.

This paper is structured as follows: In Sec. II below, we present the details of the DFT methods we have used. In Sec. III, we present our results for bulk Se, both as a benchmark for our calculations, and for later comparison with results on nanowires. Our results for the structures, binding energies, and elastic properties of nanowires are given in Sec. IV. We determine the electronic structures and densities of states, and use charge densities to probe the nature of bonding, in Sec. V. Section VI contains our results for optical conductivity, followed by conclusions in Sec. VII.

[a)]Electronic mail: mousumi@jncasr.ac.in.

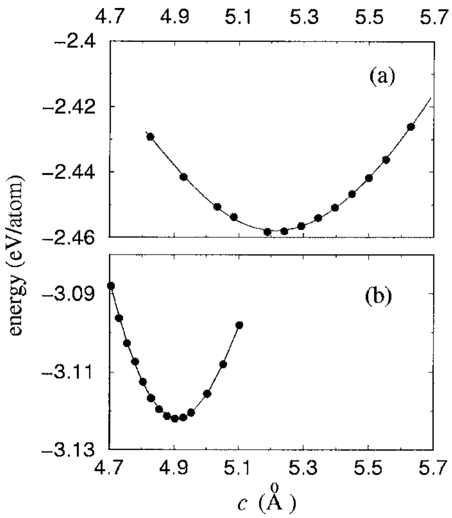

FIG. 1. Binding curves for bulk Se: the total energy per atom as a function of c, the lattice constant along z. The values of the other structural parameters a and u have been optimized for each value of c. Graphs (a) and (b) correspond to the results obtained using the GGA and LDA, respectively. The zero of energy has been chosen as the energy of the isolated atom, so that the y-axis corresponds to the negative of the cohesive energy per atom.

II. METHODS

We have performed total energy calculations using the ABINIT (Refs. 6 and 7) implementation of DFT,[8] wherein the Kohn-Sham equations[9] are solved by an iterative conjugate-gradient minimization[10] of one-electron energies in the ground state.[11] The effects of the ionic cores were approximated by using optimized norm-conserving pseudopotentials,[12] including the semicore d-states in the valence. The OPIUM (Ref. 13) code was used to construct the pseudopotential. We used a plane-wave basis with an energy cutoff of 60 Ry, and converged total energies to within 1 mRy/at.. For the exchange-correlation terms, we tried using the local density approximation (LDA),[14] using the Perdew-Zunger parametrization[15] of the Ceperley-Alder functional,[16] as well as the generalized gradient approximation (GGA) using the Perdew-Burke-Ernzerhof functional.[17–19] Brillouin zone (BZ) integrations were performed using a $5\times5\times5$ Monkhorst-Pack grid[20] (19 k-points in the irreducible BZ) in calculations for bulk Se and a $1\times1\times5$ grid (3 k-points in the irreducible BZ) for nanowires. We checked that the total energies obtained using the chosen k-point meshes are converged to within 1 mRy/at. (through selected calculations with finer meshes, for example, $1\times1\times21$, $1\times1\times8$, and $8\times8\times8$ for the single helical chain, the wire with one shell, and the bulk, respectively). To improve convergence, we used Fermi-Dirac smearing of occupation numbers of electronic states, with a smearing temperature of 474 K for bulk Se and 1137 K for the nanowires.

We present results on bulk Se (atoms per unit cell), a single helix (Se-h) with atoms per cell and a diemeter of about 5 Å, a single-shelled Se wire (Se-w1) with 21 atoms per cell and a diameter of about 13 Å, and a double-shelled Se nanowire (Se-w2) with 57 atoms per cell and a diameter of about 21 Å (however, elastic and optical properties of Se-w2 were not calculated due to computational constraints). The nanowires and helix are periodic in the c-direction but are of finite extent in the perpendicular plane; however, we used periodic boundary conditions together with hexagonal supercells, with an in-plane lattice parameter of up to 26 Å, so that a vacuum of at least 8 Å separated periodic images of the nanowires; this is sufficient to ensure that there is negligible interaction between periodic images. Structural optimizations were performed using a Broyden-Fletcher-Goldfarb-Shanno-based minimization scheme.[21]

III. RESULTS FOR BULK Se

The trigonal structure of bulk Se is characterized by three parameters: the lattice constant a in the xy-plane, the c/a ratio, where c is the lattice constant along the z-direction, and a reduced coordinate u, which specifies the position of the atoms in units of a, when the coordinates of atoms along the helices (directed along the z-axis) are projected onto the xy-plane.

We have performed a series of total-energy calculations, together with relaxations, in order to obtain the optimal values of a, c, and u. One notable feature of our results is that the numbers are extremely sensitive to the choice of exchange-correlation functional. For example, in Figs. 1(a) and 1(b), we present our results for how the total energy varies as a function of c (for optimal values of a and u), upon using the GGA and the LDA, respectively. In both cases, the zero of energy has been chosen so as to correspond to the energy of an isolated Se atom, i.e., the total energies plotted are actually the negative of the cohesive energy per atom. The features immediately obvious from a comparison of the

TABLE I. Summary of results for bulk Se: comparison of values of lattice parameters (atomic volume Ω, c/a, and internal structure parameter u), ratio of interchain and intrachain distances d_1/d_2 bond-angle θ, cohesive energy ε_c, and bulk modulus B, with results from previous calculations and experiment.

Method	Ω (Å^3)	c/a	u	d_1/d_2	θ (deg)	ε_c (eV)	B (GPa)
LDA-NC, ours	23.50	1.31	0.259	1.26	103.3	3.12	⋯
LDA-US[a]	23.16	1.30	0.259	1.26	103.0	3.36	30.40
LDA-NC[a]	23.59	1.29	0.256	1.26	103.4	3.30	⋯
PBE-NC, ours	30.07	1.157	0.229	1.42	103.2	2.46	13.72
PB-US[a]	29.11	1.159	0.224	1.43	103.4	2.56	6.9
Experimental[b]	27.28	1.136	0.229	1.50	102.5	2.25	14.9

[a]Reference 24.
[b]References 30 and 31.

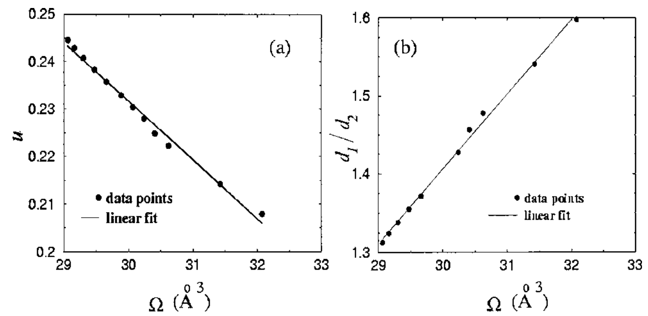

FIG. 2. Variation of internal structural parameters, for trigonal bulk Se, upon varying the atomic volume Ω: (a) reduced coordinate u, and (b) ratio of interchain bond-length d_1 to intrachain bond-length d_2.

graphs in Figs. 1(a) and 1(b) are as follows: (i) the cohesive energy is much larger with the LDA than the GGA, (ii) the atoms are more tightly packed when the LDA is used, and (iii) the curvature of the energy versus c curve (Fig. 1) is much higher for the LDA than for the GGA, implying that use of the former would lead to a higher value of Young's modulus. Note that, given the well-known tendency of the LDA to lead to overbinding, one would expect that the LDA would give a cohesive energy that is too large and an atomic volume that is too small. However, upon comparison with experiment, we find that the LDA underestimates the volume by as much as 14%, which is larger than typical LDA errors. Further, available ultrasoft pseudopotentials[22] when tested for bulk Se were found to be less suitable[23] than the norm-conserving pseudopotential used presently.

Details of the optimal values obtained by us for the various structural parameters are given in Table I, where we have also compared our results with experimental values and the results of earlier calculations on bulk Se. We have presented values for Ω, the volume per atom in the optimal structure, the c/a ratio, the value of the internal parameter u, the ratio of the interchain nearest-neighbor distance d_1 to the intrachain nearest-neighbor distance d_2, and the intrachain Se–Se–Se bond-angle θ. Our results with the LDA and GGA are described as LDA-NC and GGA-NC, respectively, with NC indicating that we have used a norm-conserving pseudopotential, and the results of an earlier study[24] using both the LDA and the Perdew-Burke GGA functional and both norm-conserving (NC) and ultrasoft pseudopotentials are also presented for comparison.

An examination of Table I shows that calculations within the GGA give better agreement with experimental values than those within the LDA. Our GGA result for u is in excellent agreement with experiment, while the GGA values of the lattice constant a and the c/a ratio are too large by about 3% and 2%, respectively. The ratio d_1/d_2 is underestimated by a very small amount of 1.4% and the error in the bond-angle θ is also negligible, corresponding to an overestimation by 0.68%. Since the GGA performs much better than the LDA for the case of bulk Se, we expect this to hold true also for the nanowires. Therefore, in the rest of this paper we only present results obtained using the GGA.

In Fig. 2, we show how u and d_1/d_2 vary as the atomic volume Ω is changed. Note that, as pointed out by previous authors,[24] the stable t-Se bulk can be related to a simple cubic structure with an atomic volume of ~ 24 Å^3, in the limit $u \rightarrow 1/3$ and $d_1/d_2 \rightarrow 1$.

IV. STRUCTURES AND ELASTIC PROPERTIES FOR Se-h, Se-w1, Se-w2, AND BULK Se

The effects of reduced dimensionality and reduced coordination are reflected in altered values for the structural parameters and elastic moduli of nanowires, relative to the bulk, as we discuss below,

A. A comparative study of structures

A summary of our results for the stability and structures of the nanowires is presented in Table II. Upon examining the structures obtained after energy minimization, we find that the structural parameter c (which is equal to the pitch of the Se helices) increases as one proceeds from the single helix towards the bulk. We obtain c=5.079, 5.170, 5.180, and 5.188 Å for Se-h, Se-w1, Se-w2, and bulk Se, respectively. From the results for the cohesive energy ε_c in Table II, one can also see that wires with increasing numbers of shells (and thus increased diameter) are progressively more stable; however, the increments in cohesive energy are quite small, suggesting that the binding between neighboring helices in the wires and bulk is quite weak.

We can define a surface energy $\gamma_s=(E_{\mathrm{NW}} - n_{\mathrm{NW}}E_{\mathrm{bulk}})/(2\pi Rc)$, where E_{NW} is the total energy of the nanowire containing n_{NW} atoms, E_{bulk} is the total energy per atom in the bulk, c is the lattice constant along the axis of the nanowire, and R is the radius of the nanowire. Note that it is not immediately obvious how to define a quantity such as the radius of a finite-extent object such as a nanowire. There are many ways of defining the radii of nanowires,[25–27] which make use of their atomic radii, bond lengths, or charge distribution. Our prescription for determining R is to compute

TABLE II. Evolution of structural and elastic parameters as one progresses from the single helical chain to the bulk: calculated values for the radius per helical chain R_h, the cohesive energy ε_c, u, the interhelical distance a, c, the bond-angle θ, the interchain to intrachain ratio d_1/d_2, and Young's modulus Y_z. For the nanowires, $R_h = R/n^{1/2}$, where n is the number of helices. Asterisks indicate average values.

System	R_h (Å)	ε_c (eV)	u	a (Å)	c	θ (deg)	d_1/d_2	Y_z (GPa)
Se-h	2.62	2.40	0.226	⋯	5.079	102.8	⋯	53.06
Se-w1	2.39	2.44	0.232*	4.439–4.506	5.17	101.3–104.9	1.43*	55.28
Se-w2	2.37	2.45	0.230*	4.443–4.501	5.18	101.8–105.1	1.43*	⋯
Se bulk	2.35	2.46	0.229	4.481	5.19	103.2	1.42	57.71

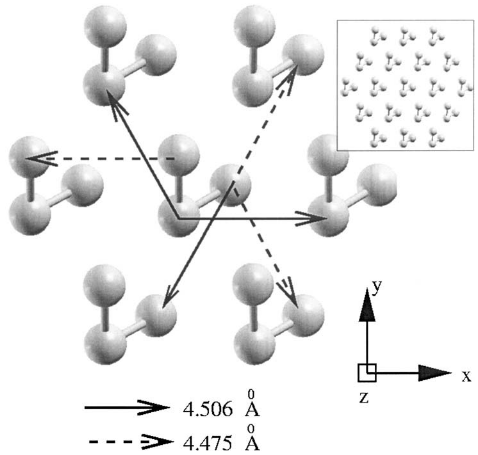

FIG. 3. Cross-sectional view of Se-w1: note that the centers of the peripheral helices do not form a perfect hexagon, but are divided into two groups of three. The inset shows the cross-sectional view of Se-w2.

the radius within which 99% of the charge is contained; while we are aware that this choice is somewhat arbitrary, we use it as an estimate to obtain quantities that seem physically reasonable, while affording a comparison with bulk properties. The values we thus obtain for γ_s are very small; we obtain values of 0.0017 eV/Å^2 (0.027 J/m^2), 0.0018 eV/Å^2 (0.028 J/m^2), and 0.0018 eV/Å^2 (0.028 J/m^2) for Se-h, Se-w1, and Se-w2, respectively.

For the bulk structure, the internal parameter u is defined in terms of the periodicity a in the xy-plane. For the nanowires, there is no periodicity in the radial plane and hence no well-defined value of a. Therefore, in order to permit comparison with the bulk, we define u for Se-h, as well as u for the central helices of Se-w1 and Se-w2, in terms of the value of a for the bulk. For the peripheral helices in Se-w1, and the helices in the first shell of Se-w2, we use a value of a that is equal to the distance between the axis of that particular helix and the axis of the central helix. For helices in the second shell of Se-w2, we define a as the distance between the axes of that particular helix and the nearest-neighbor helix in the first shell. The interchain distance d_1 is defined as the shortest distance between two atoms in two neighboring helices in the wire, while the intrachain distance d_2 is defined as the nearest-neighbor distance within a helix.

Interestingly, the effects of reduced dimensionality are reflected in a lowering of symmetry in the wires. We find that the different helices of Se-w1 are not identical, in contrast to those in the bulk. While the point symmetry of the helices at the surface of Se-w1 is the same as that of the bulk (point group of the space group $P3_221$), the centers of the helices in Se-w1 display threefold rotational symmetry about the c-axis (see Fig. 3), whereas the centers of helices in the bulk structure form a perfect hexagonal lattice. For Se-w1, the pitch and the bond angles of the central helix change in such a way that the intrachain bond lengths remain the same as in bulk Se, i.e., 2.478 Å. However, the interchain distances between the central helix and the peripheral helices d_1 change: d_1 for a set of three helices increases by 0.49% (marked by solid arrows in Fig. 3) with respect to the value for bulk Se (4.484 Å), while for the other set it decreases by 0.20% (marked by dashed arrows in Fig. 3). In all the helices, atoms are closer together in Se-w1 than in the bulk, due to the contraction of Se-w1 along the c-axis. Similar features are observed in the helices of Se-w2 (relaxed structure shown in the inset of Fig. 3; helices on the outermost shell are more affected than those in the inner shell).

B. Elastic properties of Se-h, Se-w1, and Se bulk

In order to examine the effects of dimensionality on elastic properties, we calculate Young's modulus Y, which is given by

$$Y = \frac{1}{\Omega_0}\left(\frac{\partial^2 E_t}{\partial \epsilon^2}\right)_{\epsilon=0}, \tag{1}$$

where E_t is the total energy, ϵ is the strain in the direction of deformation, and Ω_0 is the equilibrium volume of the unit cell.[28]

1. Se nanowires

The equilibrium volume in the case of cylindrical nanowires is defined as $\Omega_0=\pi R^2 c$, where R is the radius of the nanowire and c is the axial lattice constant. As mentioned above, we take R to be the radial distance within which 99% of the total number of electrons (N_e) are confined, i.e., $\int_0^R\int_0^c \rho(r)2\pi r dz dr=0.99eN_e$, where $\rho(r)$ and N_e are the charge density and total number of electrons in the system, respectively, and e is the electronic charge. Consistent with the reduction in the value of c, the radius per helix of the nanowires is found to increase with reducing diameter (see Table II). We find that for Se-h, R=2.62 Å and for Se-w1, R =6.30 Å, while the values we obtain for Young's moduli for Se-h and Se-w1 are 53.06 and 55.28 GPa, respectively.

2. Elastic stiffness constants for bulk Se

The value for Young's modulus along the z-direction, Y_z, for bulk Se, can be obtained by computing the second derivative of our curve for the total energy as a function of c. We obtain a value of 57.71 GPa, which is quite different from the experimentally reported value of 10.0 GPa.[28] Such a huge discrepancy between experimental and calculated values leads us to consider the possibility that the experimental value does not, in fact, correspond to the case of stretching along the z-axis, especially as we know that bulk Se has a very anisotropic structure. In order to further analyze the situation, we have computed elastic constants c_{ij} for bulk Se, compared them with experimental values, and checked what values they will yield for various elastic moduli. The total energy E_t can be expressed as a quadratic function of strains as follows

$$E_t = \tfrac{1}{2}c_{11}(\epsilon_{xx}^2+\epsilon_{yy}^2) + c_{12}\epsilon_{xx}\epsilon_{yy} + \tfrac{1}{2}c_{33}\epsilon_{zz}^2 + c_{13}(\epsilon_{xx}+\epsilon_{yy})\epsilon_{zz}, \tag{2}$$

where ϵ_{xx}, ϵ_{yy}, and ϵ_{zz} are strain variables and c_{11}, c_{12}, c_{33}, and c_{13} are elastic constants. Young's and bulk moduli can then be expressed in terms of these c_{ij}'s.

TABLE III. Elastic properties of bulk Se: comparison of values obtained by us with those given in the CRC Handbook, for elastic constants c_{ij}, Young's modulus Y_z, and bulk modulus B. All values are in GPa.

Calculated from	$c_{11}+c_{12}$	c_{33}	c_{13}	Y_z	B
Our results	31.3	71.1	14.6	57.35	15.66
CRC Handbook[a]	23.3	74.1	13.1	58.67	11.06

[a]Reference 32.

Young's modulus Y_z along the z-axis is obtained by minimizing E_t with respect to ϵ_{xx}, and then taking the second derivative of energy with respect to ϵ_{zz}. Thus, Y_z is given by

$$Y_z = \left(c_{33} - 2\frac{c_{13}^2}{c_{11}+c_{12}} \right). \tag{3}$$

The bulk modulus B is calculated under isotropic pressure conditions, i.e., stresses along all the principal axes should be the same, and the off-diagonal elements of the stress tensor should be zero. The stress components are found from the derivative of E_t with respect to the associated strain component. Thus, for the estimation of B,

$$\frac{\partial E_t}{\partial \epsilon_{xx}} = \frac{\partial E_t}{\partial \epsilon_{yy}} = \frac{\partial E_t}{\partial \epsilon_{zz}}. \tag{4}$$

This condition maintains the hexagonal symmetry, reducing the number of independent elastic constants, and leads to expressions for ϵ_{xx} and ϵ_{yy} in terms of ϵ_{zz}. Using this scheme, B is expressed as

$$\begin{aligned} B &= \Omega_0 \left(\frac{\partial^2 E_t}{\partial \Omega^2} \right)_{\Omega_0} \\ &= \frac{2(c_{11}+c_{12}-2c_{13})^2}{(c_{11}+c_{12}+2c_{33}-4c_{14})^2} \left(\frac{(c_{11}+c_{12})(c_{33}-c_{13})^2}{(c_{11}+c_{12}-2c_{13})^2} \right. \\ &\quad \left. + \frac{c_{33}}{2} + \frac{2c_{13}(c_{33}-c_{13})}{(c_{11}+c_{12}-2c_{13})} \right). \end{aligned} \tag{5}$$

We have performed calculations to obtain the values of the elastic constants c_{ij}. In Table III, we present our results, together with experimentally reported values.[29] We find that while our result for $c_{11}+c_{12}$ is too large, our results for c_{13} and c_{33} are in reasonable agreement with experiment. Table III also contains our results for Young's modulus and the bulk modulus, evaluated using Eqs. (3) and (5), respectively, as well as the values for Y_z and B that can be deduced from the experimental values of c_{ij}. Note that this procedure leads to theoretical and experimental values for Y_z that are now very close to each other. For the bulk modulus, there is a wide range of experimentally reported values from about 8 to 15 GPa;[28,30–32] our value is in reasonable agreement with some of these. We therefore conclude that our results for elastic constants are consistent with experimental measurements.

3. Trends in elastic constants

The results for Young's modulus presented above suggest that the wires become progressively stiffer as one goes from Se-h to the bulk. This is clearly an effect of bonding between atoms in different helices. For the single helix, there is obviously no bonding between neighboring helices, and the proportion of interhelical bonds increases as the diameter of the wires is increased until one approaches the bulk, where every helix is surrounded by six nearest-neighbor helices. Helices near the surface of a nanowire have fewer neighbors, and the corresponding absence of interhelical bonds makes the nanowires easier to stretch.

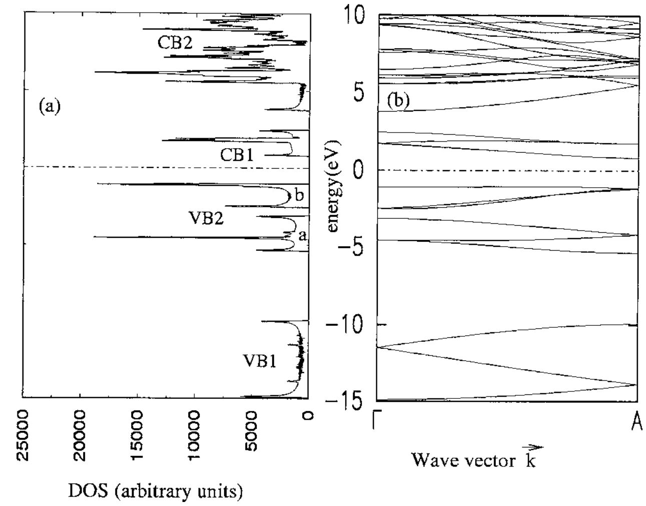

FIG. 4. (a) Density of states (DOS) and (b) electronic band structure of Se-h. The labeling of bands is explained in the text. The dot-dashed lines indicate the Fermi energy.

V. ELECTRONIC STRUCTURE

We examine the electronic structure of Se systems in order to gain a better understanding of the nature of their bonding. In Figs. 4–7, we have plotted the band structure and the electronic density of states, in the energy range from −15 to 10 eV, for Se-h, Se-w1, Se-w2, and the bulk, respectively. (Note that for the nanowires, the energies of empty states that lie significantly above the Fermi level were not computed due to computational constraints.)

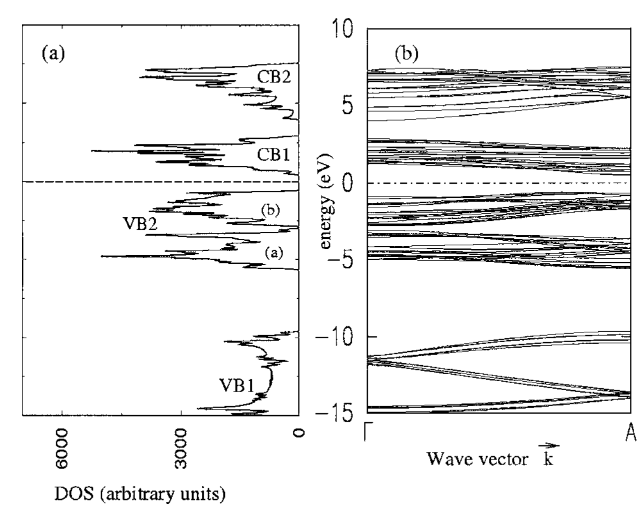

FIG. 5. (a) Density of states (DOS) and (b) electronic band structure of Se-w1. The labeling of bands is explained in the text. The dashed and dot-dashed lines indicate the Fermi energy.

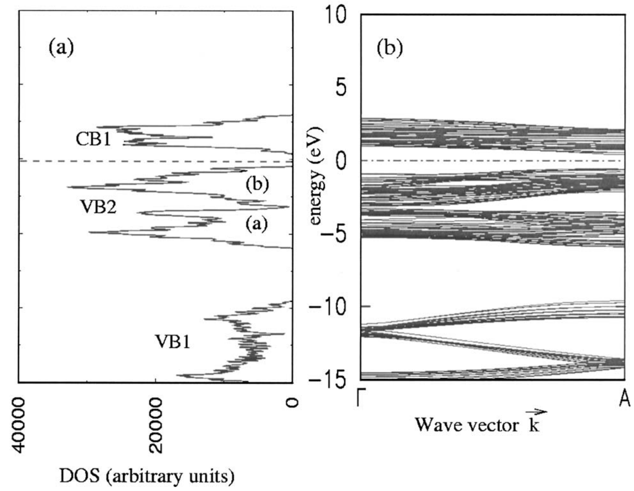

FIG. 6. (a) Density of states (DOS) and (b) electronic band structure for Se-w2. The labeling of bands is explained in the text. The dashed and dot-dashed lines indicate the Fermi energy.

For the wires, the bands are shown in the k_z-direction (which is the only periodic direction), while for the bulk, the bands are plotted along various high-symmetry directions. An examination of these graphs shows that, in all four systems, there are four principal bands, which we will denote by VB1 (first valence band), VB2 (second valence band), CB1 (first conduction band), and CB2 (second conduction band). The band VB2 appears to be composed of two subbands, which we have labeled VB2(a) and VB2(b). As we go from Se-h to the bulk, the bands clearly become broader, and all band gaps decrease. We also find that the graphs of the density of states for all the systems (see the left panels of Figs. 4–7) exhibit Van Hove singularities. We have analyzed the nature of the bonding in these four systems by projecting the charge density onto atomic orbitals. Below, we discuss the results obtained from this procedure, for each system in turn.

A. Se-h

Among the four systems, Se-h has atoms with the least number of neighbors, resulting in states that are most localized in the xy-plane, leading to the flattest bands (right panel of Fig. 4) and hence the sharpest peaks in the density of

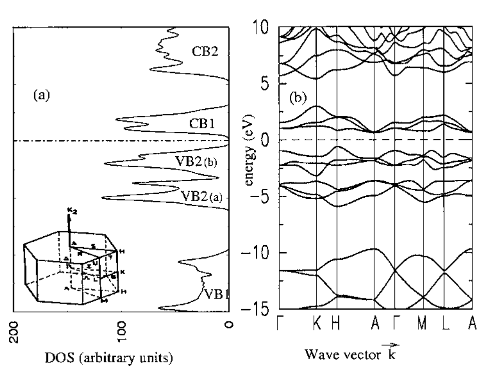

FIG. 7. (a) Density of states (DOS) and (b) electronic band structure of bulk Se along high-symmetry directions in the Brillouin zone, as indicated in the inset of panel (a). The labeling of bands is explained in the text. The dot-dashed and dashed lines indicate the Fermi energy.

states (DOS) (left panel of Fig. 4). We find that the VB1 states, between −15 and −10 eV, are predominantly s-like. They are separated by 4.8 eV from the states in the valence band VB2 (in the energy range from −5.5 to −1.0 eV), which have a mixture of p_x and p_y character, whereas the well-localized conduction bands just above the Fermi level (CB1) have a predominantly p_z-like character. There is a small energy gap of 0.7 eV at −3 eV, dividing the VB2 bands into VB2(a) and VB2(b). The s-states in VB1, being fully occupied, do not contribute significantly to bonding. For a Se atom in a helix, two bonds per atom are formed essentially by p-like states with a small admixture of s and d characters. Thus, one nonbonding p-state per atom remains. The Fermi level falls between the bonding (VB2) and nonbonding (CB1) p-states; thus, Se-h is an insulator, with a band gap of 1.82 eV. After CB1, there is a further energy gap of 2.5 eV, separating CB1 from CB2. Beyond this, there is a continuum of conduction bands (CB2) which shows about 40% p-like character, along with some admixture of d-orbitals.

B. Se-w1

The number of electrons in a unit cell of Se-w1 is 336, and at least 168 bands are needed to accommodate them. The energy levels lie very close to one another, leading to a spaghettilike band structure, as shown in the right panel of Fig. 5. As for Se-h, the VB1 states, lying between −14.5 and −9.0 eV, are found to be s-like. The Fermi level falls between bonding (VB2) and nonbonding (CB1) p-like states. The band gap of Se-w1 is found to be 0.93 eV, and thus Se-w1 is a semiconductor. Once again, VB2 shows a two-peak structure. The gap between CB1 and CB2 is also reduced to 1.3 eV. For Se-w1, the states in CB2 show a mixture of s-, p-, and d-like characters, with a dominant contribution from p-states.

C. Se-w2

The band structure for Se-w2 (see Fig. 6) is similar in its gross features to that for Se-w1, with now at least 456 bands required to accommodate 912 electrons. The gap between VB1 and VB2 is further reduced to 3.8 eV, while the band gap, between VB2 and CB1 is also reduced to 0.69 eV. Thus, like Se-w1, Se-w2 is also a semiconductor. Due to computational constraints, we did not compute high-lying empty states for Se-w2, and thus CB2 cannot be seen in Fig. 6.

D. Bulk Se

For the bulk, we have plotted the band structure (see Fig. 7) along $\Gamma \rightarrow K \rightarrow H \rightarrow A \rightarrow \Gamma \rightarrow M \rightarrow L \rightarrow A$. These high-symmetry directions of the hexagonal Brillouin zone are shown in the inset of Fig. 7(a). We find that bulk Se is a semiconductor with an indirect band gap of 0.63 eV. This is lower than the experimental band gap of 1.20 eV;[33] the underestimation of the band gap is a well-known problem with the kind of DFT calculations we have performed.

The underestimation of the energy band gap (e.g., by more than 50% for semiconducting systems) in the Kohn-

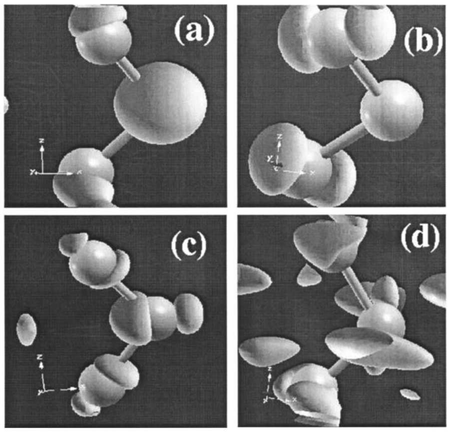

FIG. 8. Isosurfaces of charge density for bulk Se; plotted for a value corresponding to 50% of the maximum value: (a) s-like bonding for VB1, (b) mixture of p_x- and p_y-like bonding for VB2, (c) p_x-like bonding for CB1, and (d) admixture of s-, p- and d-like bonding for CB2. In all cases, the z-axis is aligned parallel to the axis of the helix shown.

Sham spectrum obtained in DFT calculations is well known to be an intrinsic shortfall of the technique. The band gap, E_g, is the minimum energy associated with an electronic excitation obtained by ignoring the interaction between the excited electron and the hole left behind (excitonic effects): $E_g=E_t(N+1)-E_t(N)+E_t(N-1)-E_t(N)$, where E_t is the ground-state energy within DFT and N the number of electrons. It can be related to the Kohn-Sham electronic eigenvalues through their interpretation as the first derivative of total energy $E(N)$ with respect to respective orbital occupancy. The first derivatives of the exact exchange-correlation functional with respect to occupation numbers are discontinuous[34] at integer N (for changes that do not conserve charge N). Hence, the estimation of the band gap from the exact Kohn-Sham spectrum always has errors that are a measure of the size of these discontinuities. In the GGA functional used here for the exchange-correlation energy, while there are no discontinuities in the functional, the incorrect treatment of the exchange-correlation and self-interaction energies leads to underestimation of the band gap. These errors translate into errors in the derived properties, such as optical conductivity, dielectric constant (also mentioned later), that depend on the band gap, which are often corrected for through a simple rigid shift in the energy of unoccupied states, called the "scissors" correction, to match the experimental band gap.[35] Note that our results for the band structure and the density of states for bulk Se display similar characteristics to those found in previous calculations.[36]

In order to shed further light on the nature of bonding, in Fig. 8 we show the isosurfaces of charge density for different bands of the bulk; similar features are observed upon examining the charge densities (not shown) for states in the corresponding bands for Se-h, Se-w1, and Se-w2. Figure 8(a) shows spherical isosurfaces with s-like character of the VB1 states. Figures 8(b) and 8(c) show, respectively, the bonding and antibonding p-like characters of states in VB2 and CB1. The CB2 states in Fig. 8(d) show a mixture of different types of orbitals.

VI. OPTICAL CONDUCTIVITY

Since selenium shows many interesting optical properties, we decided to use our results for the electronic structure to investigate optical properties. Below, we determine the optical conductivity of Se nanowires, and compare these results with those for bulk Se. The conductivity tensor σ is given by the Kubo-Greenwood formula[37,38]

$$\sigma_{\alpha\beta}(\omega)=\frac{2\pi}{3\omega}\int_{\mathrm{BZ}} dk\Sigma_{i,j}(f_i^k-f_j^k)\langle\psi_i^k|\mathbf{v}_\alpha|\psi_j^k\rangle\langle\psi_j^k|\mathbf{v}_\beta|\psi_i^k\rangle \times\delta(\epsilon_j^k-\epsilon_i^k-\omega), \tag{6}$$

where α and β are principal axis directions (which depend on the symmetry of the system), ω is the frequency, ϵ_i^k is the energy eigenvalue of the ith band at the kth k-point, f_i^k is the Fermi-Dirac occupation factor, and $\langle\psi_i^k|\mathbf{v}_{\alpha\beta}|\psi_j^k\rangle$ is the matrix element of the velocity operator corresponding to an interband transition between the bands i and j. Note that for practical evaluations of Eq. (6), the integral over the BZ is replaced by a sum over k-points, which introduces a volume factor in the expression. In the case of the nanowires, we use the real-space volume of the nanowire, rather than the supercell volume, since the latter contains also the volume of the empty vacuum regions. To compute σ, ground-state self-consistent calculations are followed by non-self-consistent calculations to determine the Kohn-Sham eigenspectrum at all the k-points of the Monkhorst-Pack grid, and three electric field response function calculations (d/dk_α calculations) to determine the derivatives of the ground-state wavefunctions with respect to k_α along three principal axes. The latter yield the velocity operator matrix elements appearing in Eq. (6). In our calculations of the conductivity and the imaginary part of the dielectric function [see Eq. (7) below], we employ a smoothening technique that replaces the delta function in Eq. (6) with a Gaussian of width=0.12 eV.

If the energy of an incident photon matches the energy of one of the Van Hove singularities in the DOS, and if the corresponding interband transition is allowed by the selection rules (obtained from the symmetry restrictions $\langle\mathbf{v}\rangle\neq 0$), a resonant enhancement in the optical conductivity is observed through a peak in $\sigma(\omega)$. In Table IV, we have given the positions of these peaks, together with information about the kind of transition they correspond to, for Se-h and Se-w1, as well as for bulk Se.

Se systems being structurally uniaxial,[39] their optical properties depend on the direction of polarization of light with respect to the c-axis (parallel to the z-direction). We have determined the zz and xx (principal) components of the optical conductivity σ; these describe the response to photons with electric field E parallel ($\parallel$) and perpendicular ($\perp$) to the c-axis, respectively. The results for the real part of σ_{xx} and σ_{zz}, at room temperature $T=300$ K, are shown in Fig. 9. (However, note that one expects these results to be redshifted with respect to the true values, because of our underestimation of the band gap; this point is discussed further below.)

Our values for the optical band gaps are essentially the same as our values for the electronic band gaps, showing that the former are not increased as a consequence of selection

TABLE IV. Transitions corresponding to the different peaks in the graph of σ_{zz}, the optical conductivity for $E \| c$.

System	Peak position (eV)	Transition
Bulk Se	1.77	
	2.67	VB2(b)→CB1
	4.62	
Se-w1	1.45	
	2.38	VB2(b)→CB1
	2.91	
	4.82	VB(a)→CB1
	5.41	
Se-h	2.06	
	2.96	VB2(b)→CB1
	4.12	
	5.03	VB2(a)→CB2

rules. In order to compare with experiments for the optical properties of the bulk,[40] we calculate the imaginary part of the frequency-dependent dielectric function, given by

$$\varepsilon_{im}(\omega) = \frac{4\pi}{\omega}\sigma^{\text{real}}(\omega). \tag{7}$$

If one simply uses this formula to evaluate $\varepsilon_{im}(\omega)$, one obtains results that show a significant redshift, as well as an enhanced magnitude, when compared with experiment;[40] see the insets to Fig. 10. The main source of this error is the underestimation of the band gap in our DFT calculations, as discussed already. The error in the band gap leads to (i) an almost rigid redshift in the spectrum described by the dielectric function or optical conductivity, and (ii) an overestimation of its magnitude, due to its inverse dependence on the gap, as seen in the Kubo-Greenwood formula for optical conductivity. The latter is similar to the overestimation of $\varepsilon_{im}^{\infty}$, the static dielectric constant.[35]

In order to account for this error, we apply the simple scissors correction,[35] whereby we raise the energy of all unoccupied states by an amount Δ that is equal to the difference between the experimental and theoretical band gaps. The main graphs in Fig. 10 show our results for $\varepsilon_{im}(\omega)$, including

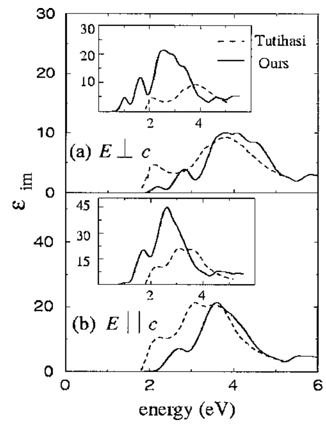

FIG. 10. Comparison of calculated (solid lines) and experimental (Ref. 40) (dashed lines) for ε_{im}, the imaginary part of the dielectric function for bulk Se, at 300 K, (a) for $E \perp c$ and (b) for $E \| c$. The main graphs show the results after applying the scissors correction, whereas the insets show the results without making this correction.

the scissors correction. It is seen that the agreement between experiment and theory is now considerably improved, to the extent possible within such a simple approach. Note also that the experimental curves presumably include contributions from processes we have neglected, such as electron-phonon interactions.[41,42]

Similarly, we can evaluate ε_{im} for the nanowires. However, as the experimental values for the band gaps of the nanowires are not known, we cannot apply the scissors correction in these cases. Therefore, in Fig. 11, we have plotted the results for Se-h, Se-w1, and the bulk, without the scissors correction in all three cases. From an examination of Fig. 10, we can expect that the true curves will be redshifted with respect to these, and also the height of the peaks will be considerably reduced.

From Figs. 9 and 11, we can draw some general conclusions on the effects of reduced diameter in the nanowires. Sharper features are seen with decreasing diameter, reflecting the narrowing of the bands. When the electric field is parallel to c, the magnitude of the optical conductivity does not vary significantly between the nanowires and the bulk; however,

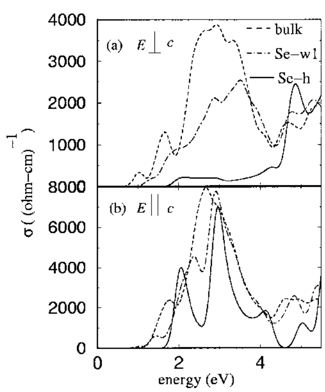

FIG. 9. The real part of the optical conductivity σ for Se-h (solid line), Se-w1 (dot-dashed line), and Se bulk (dashed line) at 300 K: (a) σ_{xx} and (b) σ_{zz} for light polarized perpendicular and parallel, respectively, to the c-axis. Note that no scissors correction has been applied.

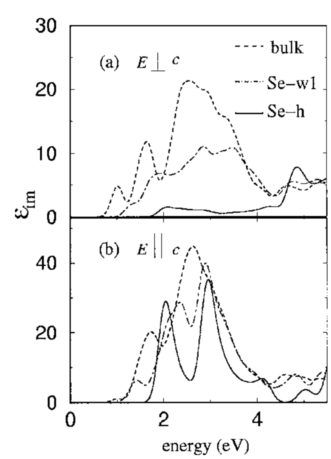

FIG. 11. Calculated values for the imaginary part of dielectric function, (ε_{im}), for Se-h (solid line), Se-w1 (dot-dashed line), and Se bulk (dashed line), at 300 K, for light polarized (a) perpendicular and (b) perpendicular to the c-axis. Note that no scissors correction has been applied.

this is not true when the electric field is perpendicular to c: the most prominent peaks in the bulk are significantly diminished in Se-w1 and absent for Se-h, suggesting that these peaks correspond to interhelical transitions. Indeed, we find that the main reason for the reduced value of conductivity when the electric field is perpendicular to c is a marked decrease in the joint density of states. However, note that for the peak that occurs between 4 and 5 eV, the ordering of magnitudes is reversed with respect to that at lower energies, i.e., the peak is highest for Se-h, followed by Se-w1 and the bulk, suggesting that this peak is due to intrachain transitions. Note also that the anisotropy in optical conductivity (which is present to some extent even in the bulk) is considerably greater in the nanowires. This suggests that aligned nanowires can be effectively used as polarizers for electromagnetic radiation in this frequency range.

VII. SUMMARY AND DISCUSSION

We have performed *ab initio* density functional theory calculations to investigate the structure, energetics, electronic structure, and elastic and optical properties of selenium nanowires and bulk. For the bulk, we find that the GGA gives very good agreement with experiments and earlier calculations, whereas the LDA performs poorly, presumably due to the fact that the charge density varies rapidly away from the helical axis.

We observe a smooth evolution of properties as one approaches the bulk, through progressively thicker nanowires, i.e., all the properties we have examined vary monotonically as one goes from Se-h to Se-w1 to Se-w2 to Se bulk.

The nanowires are found to be structurally similar to the bulk, being composed of arrays of aligned helical chains. Individual helices show very similar structures in all the cases, underlining the fact that the bonding between neighboring helices is weak. The undercoordination (with respect to the bulk structure) of atoms in the surface of the nanowires results in (a) a reduction in cohesive energy, (b) rearrangement of atoms at the surface, (c) consequent changes in the interhelical distances d by approximately 1%, (d) stronger intrahelical Se–Se bonds and decrease in the pitch of the helices (lattice parameter c) with decreasing diameter of the nanowires, and (e) decreasing values of Young's modulus, as the diameter of the nanowires is decreased. However, all these effects, though presenting a clear trend, are also small, reflecting the presence of relatively weak interchain bonding in all the cases. A detailed examination of the structure of Se-w1 clearly shows a nanosize effect: the formation of two groups of three identical peripheral (surface) helices each, consistent with its threefold rotational symmetry: interhelical distance, Se–Se bond lengths, and Se–Se–Se bond angles, is distinct for these two groups.

Though the interchain bonding is weak enough to have only a small impact on structure, increasing overlap of electronic wavefunctions of different helices with increase in the diameter of the wires results in a redshift in the band gap; we observe a noticeable change in electronic structure and optical properties as a function of the changing size of the nanowires. The bandwidths increase and band gaps decrease as one goes from the single helical chain (which is an insulator) to the bulk (which is a semiconductor). However, the nature of the bands is relatively unchanged in all the cases.

The changes in electronic band structure are reflected in the optical conductivity for photons with electric field parallel to the c-axis: the peaks are shifted slightly and become narrower as the diameter of the nanowire decreases; however, magnitudes are more or less unchanged. Strikingly, the situation is quite different when the electric field is perpendicular to the c-axis: at low to medium energies, the optical conductivity is significantly reduced for the nanowires; this effect is particularly marked for the single helix. However, at higher energies, the conductivity is actually greater for the nanowires than the bulk. For the case of Se-bulk, the values of ε_{im} calculated by us are in good agreement with experimental values, if we apply the scissors correction to compensate for the error in DFT band gaps. The optical conductivity and dielectric functions of the nanowires are more strongly dependent on the plane of polarization of light, than in the case for the bulk; this raises the possibility that bundles of aligned Se nanowires can be used as polarizers.

In general, the nanowires approach bulk behavior rather quickly (with a couple of shells of helices, with a diameter of ~2 nm), auguring well that Se nanowires with very small diameter could be used effectively in the common applications of bulk Se.

ACKNOWLEDGMENTS

We thank Professor C. N. R. Rao and Ujjal K. Goutam for useful discussions. P.G. acknowledges CSIR, India for a research scholarship. All calculations were carried out on the computing facility supported by JNCASR, Department of Science and Technology, Government of India.

[1] *Selenium*, edited by R. A. Zingaro and W. C. Cooper (Van Nostrand Reinhold, New York, 1974).
[2] Z. Y. Jiang, Z. X. Xie, S. Y. Xie, X. H. Zhang, R. B. Huang, and L. S. Zheng, Chem. Phys. Lett. **368**, 425 (2003).
[3] U. K. Gautam and C. N. R. Rao, J. Mater. Chem. **14**, 2530 (2004).
[4] X. Duan, Y. Huang, J. Wang, and C. M. Lieber, Nature (London) **409**, 66 (2001); H. M. Huang, S. Mao, H. Feick, H. Yan, Y. Wu, H. Kind, E. Weber, R. Russo, and P. Yang, Science **292**, 1897 (2001); S. W. Chung, J. Y. Yu, and J. R. Heath, Appl. Phys. Lett. **76**, 2068 (2006).
[5] J. Hu, T. W. Odom, and C. Lieber, Acc. Chem. Res. **32**, 435 (1999); S. M. Prokes and K. L. Wang, MRS Bull. **24**, 13 (1999); Z. L. Wang, Adv. Mater. (Weinheim, Ger.) **12**, 1295 (2000).
[6] X. Gonze, J. M. Beuken, R. Caracas, F. Detraux, M. Fuchs, G. M. Rignanese, L. Sindic, M. Verstraete, G. Zerah, F. Jollet, M. Torrent, A. Roy, M. Mikami, P. Ghosez, J. Y. Raty, and D. C. Allan, Comput. Mater. Sci. **25**, 478 (2002), URL: http://www.abinit. org
[7] S. Goedecker, J. Siam, SIAM J. Sci. Comput. (USA) **18**, 1605 (1997).
[8] P. Hohenberg and W. Kohn, Phys. Rev. **136**, 864B (1964).
[9] W. Kohn and L. J. Sham, Phys. Rev. **140**, 1133A (1965).
[10] M. C. Payne, M. P. Teter, D. C. Allan, T. A. Arias, and J. D. Joannopoulos, Rev. Mod. Phys. **64**, 1045 (1992).
[11] X. Gonze, Phys. Rev. B **54**, 4383 (1996).
[12] A. M. Rappe, K. M. Rabe, E. Kaxiras, and J. D. Joannopoulos, Phys. Rev. B **41**, 1227 (1990).
[13] URL: http://opium.sourceforge.net/guide.html
[14] S. Goedecker, M. Teter, and J. Huetter, Phys. Rev. B **54**, 1703 (1996).
[15] J. P. Perdew and A. Zunger, Phys. Rev. B **23**, 5048 (1981).
[16] D. M. Ceperley and B. J. Alder, Phys. Rev. Lett. **45**, 566 (1980).
[17] J. P. Perdew, K. Burke, and M. Ernzerhof, Phys. Rev. Lett. **78**, 1396 (1997).

[18] Y. Zhang and W. Yang, Phys. Rev. Lett. **80**, 890 (1998).
[19] J. P. Perdew, K. Burke, and M. Ernzerhof, Phys. Rev. Lett. **80**, 891 (1998).
[20] H. J. Monkhorst and J. D. Pack, Phys. Rev. B **13**, 5188 (1976).
[21] http://www.library.cornell.edu/nr/bookcpdf/c10-7.pdf
[22] S. Baroni, A. D. Corso, S. Gironcoli, and P. Giannozzi, http://www.pwscf.org
[23] For example, upon using the open source GGA ultrasoft pseudopotential Se.pbe-van.UPF for bulk Se, the atomic volume Ω was found to be overestimated by 12%, and the reduced coordinate u underestimated by 9%, with respect to experiment.
[24] G. Kresse, J. Furthmuller, and J. Hafner, Phys. Rev. B **49**, 13181 (1994), and references therein.
[25] K. Nakamura and A. Ikawa, Phys. Rev. B **66**, 024306 (2002).
[26] E. Hernandez and A. Rubio, Newsletter **32**, 48 (1999); http://psi-k.dl.ac.uk/newsletters/News_32/newsletter_32.pdf.
[27] M. Cococcioni, F. Mauri, G. Ceder, and N. Marzari, Phys. Rev. Lett. **94**, 145501 (2005).
[28] URL: http://www.webelements.com/webelements/elements/text/periodic-table
[29] *Handbook of Chemistry and Physics*, 79th ed, edited by D. R. Lide (CRC, Boca Raton, FL, 1998).
[30] D. R. McCann and L. Cartz, J. Appl. Phys. **43**, 4473 (1972); W. Lingelbach, J. Stuke, G. Weiser, and J. Trensch, Phys. Rev. B **5**, 243 (1972).
[31] C. Kittel, *Introduction to Solid State Physics*, 5th ed. (Wiley, New York, 1976), p. 74.
[32] J. Mort, J. Appl. Phys. **38**, 3414 (1967).
[33] S. J. Clark, G. J. Ackland, and H. Akbarzadeh, Phys. Rev. B **56**, 329 (1995).
[34] L. Sham and M. Schluter, Phys. Rev. Lett. **51**, 1888 (1983).
[35] Z. H. Levine and D. C. Allan, Phys. Rev. Lett. **63**, 1719 (1989).
[36] J. D. Joannopoulos, M. Schluter, and M. L. Cohen, Phys. Rev. B **11**, 2186 (1975).
[37] R. Kubo, J. Phys. Soc. Jpn. **12**, 570 (1957).
[38] D. A. Greenwood, Proc. Phys. Soc. London **71**, 585 (1958).
[39] J. S. Blakemore, D. Long, K. C. Nornura, and A. Nussbaum, *Progress in Semiconductors* (Wiley, New York, 1962), Vol. 6, p. 38.
[40] S. Tutihasi and I. Chen, Phys. Rev. **158**, 623 (1967).
[41] X. Gonze, Phys. Rev. B **55**, 10337 (1997).
[42] E. W. Wong, P. E. Sheehan, and C. M. Lieber, Science **277**, 1971 (1997).